Cytotoxicity of Recombinant Tamapin and Related Toxin-Like Peptides on Model Cell Lines

ARTICLE *in* CHEMICAL RESEARCH IN TOXICOLOGY · MAY 2014

Impact Factor: 3.53 · DOI: 10.1021/tx4004193 · Source: PubMed

9 AUTHORS, INCLUDING:

Yanis Toledano-Magaña

Universidad Nacional Autónoma de México

8 PUBLICATIONS **14** CITATIONS

SEE PROFILE

Patricia Cano-Sánchez

Universidad Nacional Autónoma de México

15 PUBLICATIONS **208** CITATIONS

SEE PROFILE

Luis G Brieba

Center for Research and Advanced Studies of t…

51 PUBLICATIONS **692** CITATIONS

SEE PROFILE

Federico Del Río

Universidad Nacional Autónoma de México

40 PUBLICATIONS **475** CITATIONS

SEE PROFILE

Chemical Research in Toxicology

Article

pubs.acs.org/crt

Cytotoxicity of Recombinant Tamapin and Related Toxin-Like Peptides on Model Cell Lines

Belén Ramírez-Cordero,[†] Yanis Toledano,[‡] Patricia Cano-Sánchez,[†] Rogelio Hernández-López,[†,∥] David Flores-Solis,[†] Alma L. Saucedo-Yáñez,[†] Isabel Chávez-Uribe,[†] Luis G. Brieba,[§] and Federico del Río-Portilla*[,†]

[†]Instituto de Química, Universidad Nacional Autónoma de México, Ciudad Universitaria, Circuito Exterior s/n, México, D.F. 04510, México

[‡]Instituto de Ciencias Biomédicas, Universidad Nacional Autónoma de México, Ciudad Universitaria, Circuito Exterior s/n, México, D.F. 04510, México

[§]Laboratorio de Genómica para la Biodiversidad, CINVESTAV Unidad Irapuato, Km. 9.6 Libramiento Norte Carr. Irapuato-León 36821, Irapuato Gto, México

Supporting Information

ABSTRACT: The scorpion toxin tamapin displays the most potent and selective blockage against KCa2.2 channels known to date. In this work, we report the biosynthesis, three-dimensional structure, and cytotoxicity on cancer cell lines (Jurkat E6-1 and human mammary breast cancer MDA-MB-231) of recombinant tamapin and five related peptides bearing mutations on residues (R6A,R7A, R13A, R6A-R7A, and GS-tamapin) that were previously suggested to be important for tamapin's activity. The indicated cell lines were used as they constitutively express KCa2.2 channels. The studied toxin-like peptides displayed lethal responses on Jurkat T cells and breast cancer cells; their effect is dose- and time-dependent with IC_{50} values in the nanomolar range. The order of potency is r-tamapin > GS-tamapin > R6A > R13A > R6A-R7A > R7A for Jurkat T cells and r-tamapin > R7A for MDA-MB-231 breast cancer cells. Our structural determination by NMR demonstrated that r-tamapin preserves the folding of the αKTx5 subfamily and that neither single nor double alanine mutations affect the three-dimensional structure of the wild-type peptide. In contrast, our activity assays show that changes in cytotoxicity are related to the chemical nature of certain residues. Our results suggest that the toxic activity of r-tamapin on Jurkat and breast cancer cells could be mediated by the interaction of charged residues in tamapin with KCa2.2 channels via the apoptotic cell death pathway.

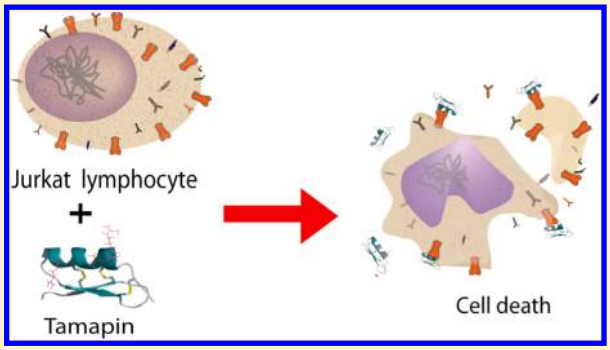

INTRODUCTION

Toxins are the major constituent of scorpion venoms. They are known for their blocking and regulatory activity on ion channels.[1−4] Tamapin, also known as αKTx5.4 and originally isolated from the venom of the *Mesobuthus tamulus* scorpion, is one of the very few selective toxins.[5] It belongs to the αKTx5 toxin subfamily, characterized by a cystine-stabilized α/β scaffold (CS-α/β) that comprises an α-helix and a double-stranded β-sheet connected by two highly conserved disulfide bridges (C2−C5 and C3−C6) and another disulfide bridge between cysteines C1−C4. Tamapin is a selective blocker of small conductance calcium activated potassium channels (KCa2). Three KCa2 subtypes have been identified up to date: KCa2.1−KCa2.3 (tamapin has IC_{50} = 42 nM, 24 pM, and 1.7 nM for KCa2.1, KCa2.2, and KCa2.3 respectively[5]). These channels are thought to be important regulators of excitability and synaptic plasticity[6,7] and display partial overlap with distinct locations in the central and peripheral nervous systems. On the basis of their activity and distribution, KCa2 channels have been proposed as novel targets for cognitive enhancement, depression, myotonic muscular dystrophy, and heart arrhythmias.[8] Previous studies have proposed molecular motifs that could be responsible for tamapin's affinity to KCa2 channels.[9] The subfamily αKTx5 is characterized for having important interacting amino acids in the α-helix, specifically in the conserved RXCQ motif,[10−12] whereas the interacting residues in the KCa2 channels are located in the extracellular loop DQQD motif.[9,13,14]

A theoretical study suggested that the main interactions for the binding of tamapin to human KCa2.2 channels are given by four hydrogen bonds that involve the tamapin residues Arg6, Arg13, and Tyr31 as well as several electrostatic interactions through residues Arg13, Arg7, and Lys20.[15]

Despite its high homology with other members of the αKTx5 toxin subfamily (Figure 1A), tamapin is the most potent and

Received: November 11, 2013
Published: April 30, 2014

   dx.doi.org/10.1021/tx4004193 | *Chem. Res. Toxicol.* 2014, 27, 960−967

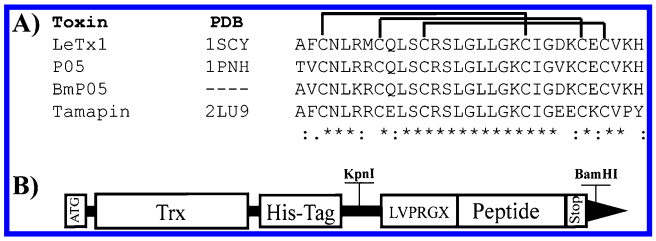

Figure 1. (A) Amino acid sequence alignment of some members of the α-KTx5 subfamily and related peptides. Alignment was performed using MAFFT software. The asterisk (*) indicates that amino acid residues in that column are conserved among aligned peptide amino acid sequences; (:) and (.) indicate conserved and partially conserved residue substitutions, respectively. (B) Construction of the fusion protein, the thrombin cleavage site LVPRGX, where X = Ser or Met, was designed to produce GS-peptides or GM-peptides.

selective toxin against KCa2.2 channels.[16] Since there was no structural information on tamapin until now, we sought to perform a structure−activity study of tamapin and several derivative peptides in order to analyze the structural basis of tamapin's toxic activity on cells that express KCa2.2 channels. We report here the cytotoxicity of tamapin and several peptides where one or two arginine residues were replaced by alanine (mutants R6A, R7A, R13A, and R6A-R7A). We utilized Jurkat and MDA-MB-231 cells as they express KCa2.2 channels constitutively;[17,39] the similar activity observed for the indirectly tested toxins increases the likelihood of the observed effects being due to an action on KCa2.2 channels. Additionally, our combined activity assays and NMR structural analysis suggest that the toxicity of the tested peptides is mediated by the interaction of charged residues in the toxin with residues in KCa2.2 channels. We also compare the cytotoxicity of tamapin and its mutants with apamin, which is a well-known KCa2 channel blocker commonly used to identify the currents of this family of channels.[7]

MATERIALS AND METHODS

Gene Cloning. Tamapin's gene was designed based on the amino acid sequence previously reported[5] and codon-optimized for *E. coli* expression. Two expression plasmids were constructed by inserting a thrombin cleavage amino acid coding sequence (LVPRGS or LVPRGM) and the tamapin sequence between *Kpn*I and *Bam*HI restriction sites in a pET32a plasmid (Novagen) (Figure 1B). The LVPRGS thrombin cleavage site produces peptides with two residues (Gly-Ser) in the amino termini (GS-peptides) because hydrolysis of the peptide bond is performed between the arginine and glycine residues. The LVPRGM thrombin cleavage site produces GM-peptides, which are designed to obtain the native sequence (r-tamapin) after the removal of the GM residues using CNBr. Mutants r-R6A, GS-R7A, r-R13A, and r-R6A-R7A were obtained by point mutations using these plasmids as templates. All vectors were verified by DNA sequencing (Laragen Inc.) using T7 prom and term primers.

Protein Expression. Fusion proteins were overexpressed in *E. coli* Rosetta gami (DE3) pLysS (Novagen, Madison WI) transformed with the corresponding vector. Overnight cultures grown at 37 °C in LB media (Sigma-Aldrich unless otherwise specified) were diluted 1:100 in fresh media containing 100 μg/mL ampicillin, 32 μg/mL chloramphenicol, 15 μg/mL kanamycin, and 12 μg/mL tetracycline. Protein expression was induced with IPTG (GoldBio) at a final concentration of 0.5 mM when OD600 nm reached between 0.6 and 0.7. Cells were incubated for 8 h at 30 °C and then harvested by centrifugation at 6000*g* for 10 min.

Protein Purification. The cellular pellet was resuspended in lysis buffer (150 mM NaCl and 50 mM Tris-HCl, pH 8) and sonicated using a Misonix Sonicator 3000 (10 min total process time, 60 W). The soluble fraction was separated by centrifugation at 32000*g* for 45 min at 4 °C. Soluble fusion proteins were isolated by IMAC using a HiTrap Ni^{2+} column (GE Healthcare) and eluted with two column volumes of elution buffer (50 mM Tris-HCl, 150 mM NaCl, and 500 mM imidazole, pH 8). Fusion proteins were treated with thrombin. The reaction was carried out at room temperature for 4 h in cleavage buffer (50 mM Tris-HCl and 10 mM $CaCl_2$, pH 8). Products were purified by IMAC to remove fusion protein residues. The flow through containing either GS-peptides or GM-peptides was desalted using a PD10 column (GE Healthcare) and purified at room temperature by RP-HPLC using a Pro-Star Varian instrument. Separation was performed using a C18 semipreparative column (Phenomenex; Jupiter,

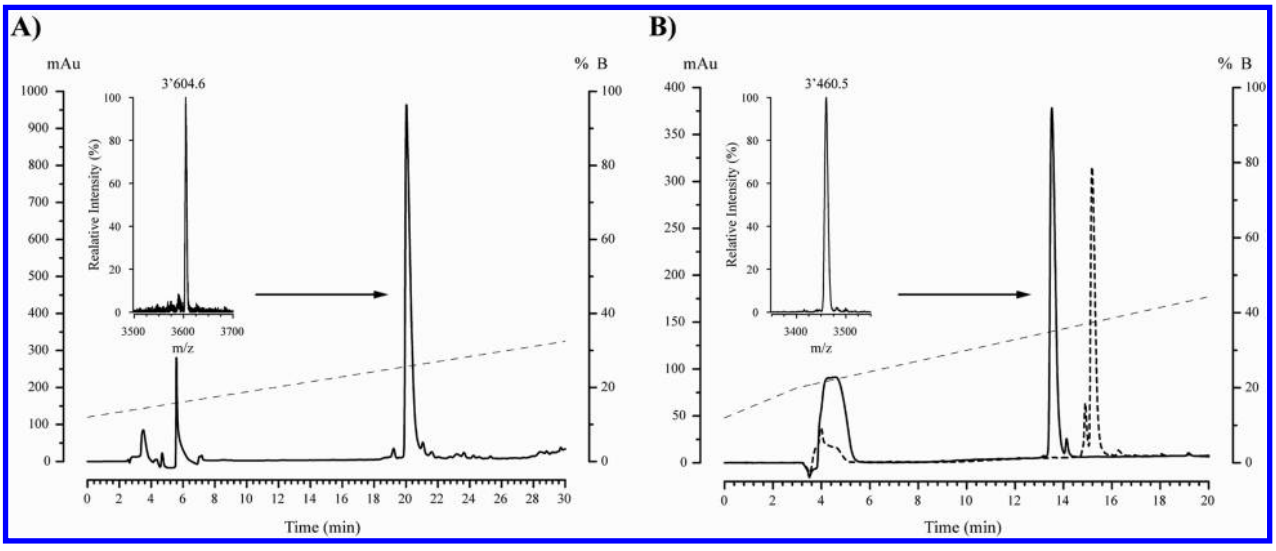

Figure 2. (A) Purification by reverse phase HPLC in a Jupiter column (Phenomenex) and MALDI-TOF characterization of GS-tamapin. (B) Chromatograms of GM-tamapin (dotted line) and r-tamapin (continuous line) in a Proteo column (Phenomenex) and MALDI-TOF spectra of r-tamapin. Purifications were performed using gradients of solution A (TFA 0.05% in H_2O) and solution B (TFA 0.05% in acetonitrile). Gradients are indicated in dotted gray lines. In B, a retention time difference of approximately 1.5 min between GM-tamapin and its product of hydrolysis with CNBr (r-tamapin) is shown.

dx.doi.org/10.1021/tx4004193 | *Chem. Res. Toxicol.* 2014, 27, 960−967

100 × 21.2 mm, 10 μm particle diameter; 300 Å pore size) equipped with a C18 guard column (Phenomenex, Jupiter, 50 × 10 mm, 10 μm particle diameter; 300 Å pore size). Elution was conducted at 10 mL/min, using solutions A (0.05% (v/v) aqueous TFA) and B (0.05% (v/v) TFA in MeCN). A nonlinear gradient from 10% to 30% solution B during 30 min was used. Peptide absorbance was monitored at 230 nm. An analytic C18 column (Phenomenex; Jupiter, 250 × 4.6 mm, 3 μm particle diameter; 300 Å pore size) was used for the evaluation of samples; chromatograms are shown in Figure 2; solutions A and B were used as the mobile phase. The collected fraction was lyophilized. Obtaining of peptides without GM residues in the N termini required two additional steps: the hydrolysis of GM-residues with CNBr (an acutely toxic compound) according to Zhao et al.[18] and a second separation by RP-HPLC with the above-described conditions.

Mass Spectrometry. MALDI-TOF on a Bruker Daltonics Microflex LT equipment was used to determine the molecular mass of the proteins. Data were acquired in the m/z range of 2000−8000 using the reflector operation mode acquiring 150 shots. Samples were prepared with α-cyano-4-hydroxycinnamic acid in a 1:10 ratio following a protocol previously reported.[19]

NMR Data Acquisition and Analysis. Lyophilized peptides were dissolved at a concentration between 1.0 and 2.8 mM in H_2O and 5% (v/v) D_2O (Cambridge Isotopes Laboratories). NMR data were acquired at 297 K using a Varian Inova spectrometer operating at 500 MHz proton frequency. NMR experiments were recorded with 1024 data point matrices using 32 scans and conducted using the DPFGSE method for water suppression;[20] DQF-COSY and TOCSY isotropic mixing time of 75 ms; NOESY mixing times of 100, 200, and 300 ms. NMR data were processed using NMRPipe;[21] and a sine window function, baseline correction, zero filling, and a second baseline correction were applied prior to Fourier transformation. Identification of amino acid spin systems and assignment of NOE signals were achieved using a CARA1.5 NEASY application.[22]

Structure Calculation. Identification of amino acid spin systems and sequential assignment were done using the standard strategy described by Wagner and Wüthrich.[23] Spin systems were identified using TOCSY and DQF-COSY spectra. Sequential assignments were obtained from an analysis of HN−HN, HN−Hα, and HN−Hβ connectivities in NOESY spectra using mixing times of 300 and 200 ms. All 1HN atoms but the one of residue 1 were assigned. Distance and dihedral angle constraints were mainly derived from cross-peaks in NOESY experiments (mix = 100 or 150 ms) using CYANA 2.1.[24,25] For each peptide, a total of 200 structures were calculated, and 20 were selected on the basis of the CYANA target function. Structures of r-tamapin, GS-tamapin, and mutants were refined using AMBER 9.[26−28] All of the molecular dynamics simulations and the energy minimizations described here were carried out using the topology and force field parameter of AMBER-99SB force field.[29] We followed the refinement protocol proposed by Gurrola and co-workers.[30] Structure evaluation was performed with the PROCHECK utility in the Validation Server of Protein Data Bank; see the Ramachandran plot in Supporting Information, Figure S2.

Cell Culturing. Jurkat E6-1 and MDA-MB-231cells were grown in RPMI 1640 with L-glutamine medium (RPMI 1640, GIBCO) supplemented with 10% of fetal bovine serum (FBS, GIBCO) and 1% of gentamicin (Gentamicin sulfate 50 mg/mL, Biosera) for 72 h. Briefly, 3 × 10^5 cells/well were plated in a 96-well microplate with supplemented RPMI medium in the presence of the toxins at four different concentrations (0.1, 1, 10, and 100 nM).

Human Peripheral Blood Lymphocytes Isolation. Buffy coats of human peripheral blood (HPB) were used to isolate lymphocytes using a density gradient of Ficoll-Paque. Ten milliliters of buffy coats were diluted with the same volume of PBS (phosphate buffer solution) then put over 12 mL of Ficoll-Paque. First, centrifugation was carried out at 690g for 25 min; subsequently, the leucocytes were absorbed with a Pasteur pipet and washed with cold PBS. Finally, the cells were counted, and 1 × 10^6 cells were plated in Petri dishes with supplemented RPMI1640 medium. After 4 h, the supernatant was transferred to new or clean Petri dishes to eliminate the adhered cells. After 24 h of growth, this procedure was repeated, and the lymphocytes in the supernatant were counted. Three ×10^5 cells/well were plated in 96-well microplates with supplemented RPMI medium in the presence of the toxins at four different concentrations (0.1, 1, 10, and 100 nM).

Viability Assay. Viability was assessed employing two different methods: (1) vital marker trypan blue and (2) carboxyfluorescein diacetate (CFDA) and propidium iodide fluorescent markers. The viability counts at 0, 6, 12, 24, 30, and 36 h were determined. For the viability assays, 3 wells were used for each time and concentration of toxin. At each time evaluated, the content of each well was homogenized and divided into two Eppendorf tubes. One of the tubes was stained with trypan blue and the other one with CFDA and PI. Cell count using fluorescent dyes was done in a fluorescent microscope Olympus BX51, whereas the count using trypan blue was carried out in a neubauer chamber taking 10 μL of each previously stained sample. Each sample was counted three times, averaged, and referred to as 1 count. Staining with trypan blue allows the observation of the morphology of the cells, while the fluorescent stain gives information about whether the cells have cytosolic activity for the presence of active descarboxylases. The number of counted living cells in the control sample was always considered the one with 100% of viability, and it was considered that the death cells were never more than 5% for cancer cells. Three independent experiments in triplicate were performed for each concentration, giving 9 data sets for each staining method. Thereby, a total of 18 data sets were averaged for each point in Figure 4. Cells without toxins were used as a negative control. Additionally, lymphocytes of human peripheral blood were employed as a second negative control, and apamin (purified from bee venom by Sigma-Aldrich) treatment was used as the positive one. All controls were also made in triplicate. Cytotoxicity data were blank corrected and normalized to the vehicle control (%viability) using a two way ANOVA significant statistical difference with a 95% confidence interval. IC_{50} values were calculated with a Probit model (Stat Graph v2.0, 2010). The program does a linear regression with the percentage of cell viability as a concentration function. The IC_{50} value is then estimated using the fitted line $y = mX + bX$, meaning $IC_{50} = (0.5 - b)/m$ with a confidence interval of 95%.

Mechanism of Cell Death. To determine the mechanism of cell death, flow cytometry analysis was done employing the FITC Annexin V Apoptosis Detection Kit with PI (Biolegend, USA) according to the protocol provided. Briefly, cells were washed with PBS solution and resuspended in the kit buffer at a concentration of 0.5 × 10^7 cells/mL. Then, 100 μL of cell suspension was placed in a flow cytometry tube; and 5 μL of FITC annexin V and 10 μL of propidium iodide solution were added. After 15 min of incubation at room temperature (25 °C) without light, 400 μL of annexin V binding buffer was added to each tube, and the samples were finally analyzed by flow cytometry in a FACScan flow cytometer (BD, USA).

RESULTS AND DISCUSSION

Toxin Expression and Purification. We report the production of r-tamapin and several mutants using the heterologous expression system *E. coli* Rosetta gami/pET32a. The single and double mutants had higher yields than the wild type protein. Our purification strategy provided acceptable yields (1.5−2.8 mg/L, Table 1) for this kind of toxin that

Table 1. Mass Characterization by MALDI-TOF

peptide	MALDI mass of $[M + 1]^+$	theoretical mass	yield (mg/L) $[M \times 10^{-3}]$
r-tamapin	3460.5	3459.1	1.5 [4.3]
GS-tamapin	3604.6	3603.2	1.7 [4.7]
r-R6A	3375.3	3374.05	2.0 [5.9]
GS-R7A	3519.5	3518.2	2.0 [5.6]
r-R13A	3375.4	3374.05	1.8 [5.3]
r-R6A-R7A	3290.1	3288.9	2.8 [8.5]

dx.doi.org/10.1021/tx4004193 | Chem. Res. Toxicol. 2014, 27, 960−967

allowed us to perform structural and functional analyses. The desired fusion proteins localized in the soluble cellular lysate were efficiently retained by a HiTrap Ni^{2+} column. Hydrolysis with thrombin was quantitative, and the Trx-His6-LVPR residue was satisfactorily removed from the reaction mixture by a second IMAC isolation. Purification of the nonretained fraction was performed by RP-HPLC (Figure 2A). The chromatogram presents only one major peak suggesting that the expression system favors a unique product; GM-tamapin elutes at 15.2 min. After hydrolysis of GM-tamapin with CNBr, the product (r-tamapin) has a retention time of 13.5 min in similar conditions; the retention time decrement is consistent with the loss of two residues. Analysis of chromatographic profiles, shown in Figure 2B, allowed us to conclude that (a) the conditions allow a clear separation between GM-tamapin and r-tamapin and that (b) CNBr hydrolysis under our working conditions was quantitative. Our mass determination is in good agreement with theoretical data (ProtParam tool from ExPASy server[31]) calculated for peptides containing three disulfide bonds (see Table 1). In contrast to the native peptide, the recombinant wild-type peptide and its mutants lack the amidation cap in their carboxyl termini. IC_{50} values for nonamidated tamapin are not available in the literature, and the importance of this posttranslational modification has only been reported for apamin.[32]

NMR Structures. Similar to other members of the αKTx5 toxin subfamily,[12,33] our structures show the characteristic secondary structure elements: one stretch of α-helix (Leu5-Ser14) connected by a turn to a β-sheet formed by two antiparallel strands (strand I, Leu18-Ile22; and strand II, Glu25-Pro30). NMR distance constraints used for each peptide are listed in Table 2. A cartoon representation of the determined three-dimensional structure of r-tamapin is shown in Figure 3A. The best structure of r-tamapin overlaps without significant changes with the structure of other members of the αKTx5 family (Figure 3B). The RMSD of the backbone after alignment of leiurotoxin, P05, and r-tamapin is 0.75 Å, which is similar to the RMSD of the r-tamapin experimental ensemble. Our structural comparison let us conclude that our expression system provides r-tamapin with its native folding. In addition, we found that mutating arginine residues, which were suggested to be important for tamapin's activity, does not affect its tertiary structure. Figure 3C shows an ensemble of all our studied peptides after alignment of the structures with the lowest CYANA target function values, which were refined by molecular dynamics with minimal distance violations.

Table 2. Final Set of NOEs Included in the Structures Calculated by CYANA

	r-tamapin	GS-tamapin	GS-R6A	GS-R7A	GS-R13A	GS-R6A-R7A
			Upper Distance Limits			
total	301	414	458	524	446	517
short range	220	262	290	312	280	301
medium range	44	80	83	115	90	108
long range	37	72	85	97	76	108
			RMSD			
average backbone (Å)	0.75	0.35	0.51	0.72	1.05	0.88

Cytotoxicity Assays. We used three different cell types to study the effect of tamapin's activity on KCa2.2 channels as an indirect measure, evaluating the viability of cell culture. Two of them, Jurkat T cells and MDA-MB-231, constitutively express these channels, whereas the other, HPB lymphocytes, does not. The membrane potential of HPB lymphocytes is supported by voltage-gated, depolarization activated Kv1.3 and Ca^{2+} activated KCa3.1 K^+ channels.[34] Purified peptides were tested at four concentrations (0.1, 1, 10, and 100 nM) and five exposure time points (6, 12, 24, 30, and 36 h) on both cell types to study the effect of tamapin's activity on KCa2.2 channels as an indirect measure, evaluating the viability of cell culture. On HPB lymphocyte cultures, all peptides produced a dose- and time-dependent effect but with low toxicity (viability ranges from 80 to 88% with the maximum toxin concentration at 38 h) in the concentration range assayed. The results are in accordance with the absence of KCa2.2 channels in these cells. In contrast, on Jurkat T cells, the peptides displayed mainly a dose-dependent effect and significant toxicity even at the lower toxin concentration (0.1 nM) during the first 6 h. All results are shown in Figures 4 and S1 (Supporting Information). Longer exposure time did not produce a viability decrease at low peptide concentration; however, all peptides have a time-dependent effect. We found higher cytotoxicity at 100 nM (32−37% viability at 6 h and 16−24% viability at 38 h); peptides with GS residues at their amino termini displayed the largest effect. Apamin, GS-tamapin, and r-R6A-R7A showed a biphasic effect on the viability of Jurkat E6-1 cells, increasing their toxicity after 24 h at 100 nM as shown in the viability graphs (Figures 4B and S1A and S1E (Supporting Information). This effect might be caused by desorption of toxins from

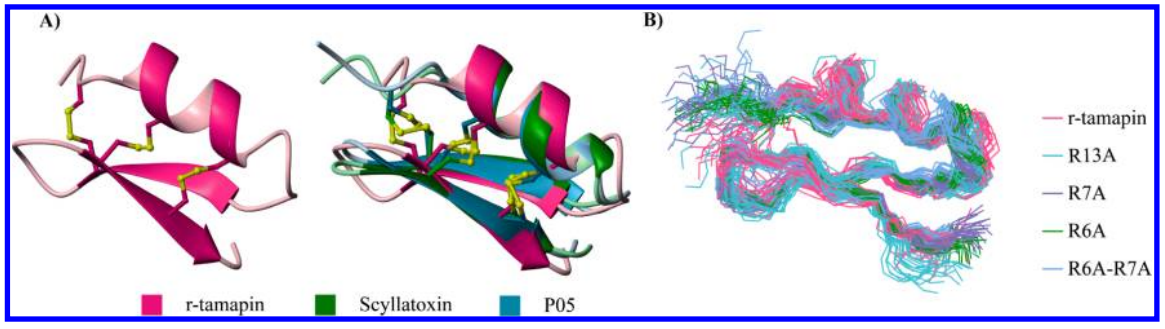

Figure 3. (A) Cartoon representation of the three-dimensional structure determined by 1H-NMR of the r-tamapin produced using the expression system reported in this article. (B) Superposition of three-dimensional structure determined for r-tamapin and previously reported structures of leiurotoxin and P05. RMSD was determined considering a total of 60 structures (20 structures by peptide). (C) Superposition of the ensembles of five peptides produced in this work. The GS tag is not plotted in this representation.

dx.doi.org/10.1021/tx4004193 | Chem. Res. Toxicol. 2014, 27, 960−967

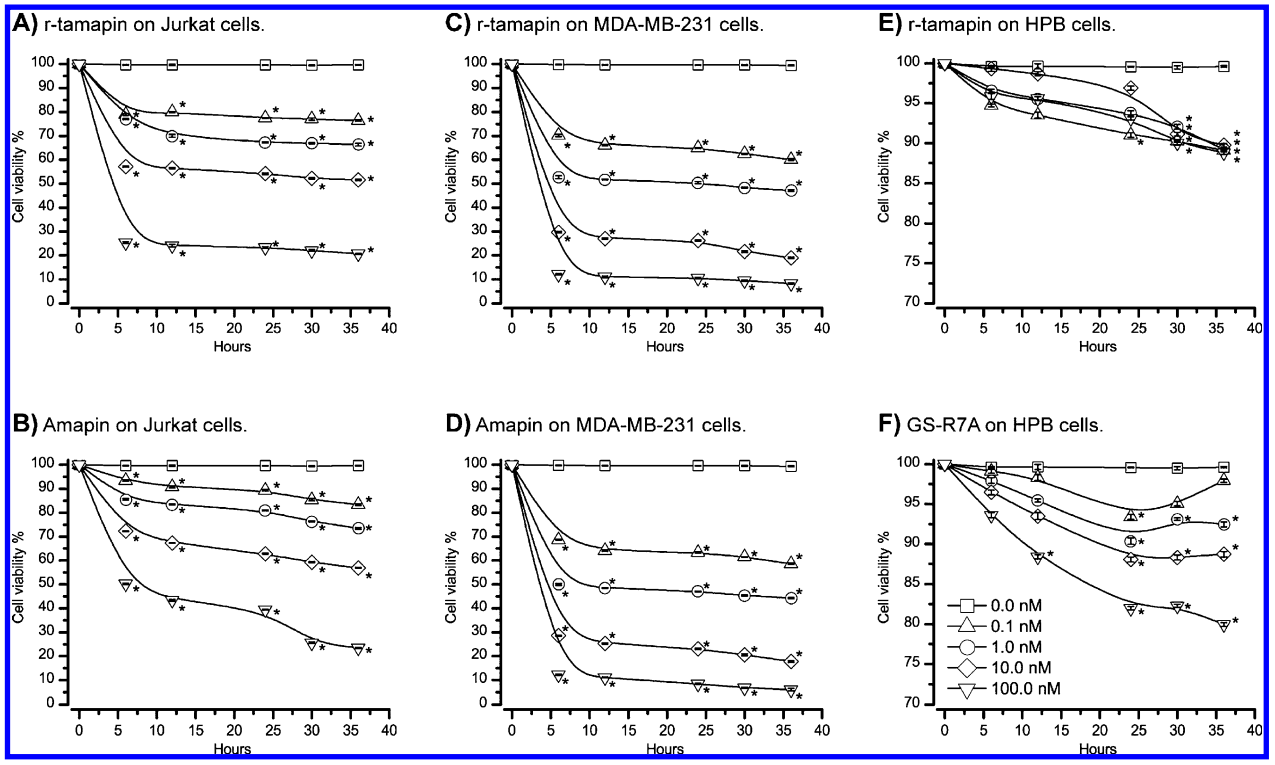

Figure 4. Viability graphs of Jurkat lymphocytes and MDA-MB-231 cells treated with 0.1, 1, 10, and 100 nM of r-tamapin and apamin. Viability graphs of human peripheral blood lymphocytes treated with r-tamapin and GS-R7A. Data are shown as the percentage of viable cells and represent the mean ± SD of three independent assays which were made by triplicate measurements. Significant differences between treated cells and controls ($p < 0.05$) are represented with an *. Viability assays of r-tamapin on both Jurkat (A) and MDA-MB-231 cells (C) displayed similar behavior, with a remarkable effect at the first 6 h and minimal changes during the next 30 h. Apamin's effect on MDA-MB-231 (D) cells have similarity with the effect of r-tamapin on this cells; however, there is biphasic behavior at 100 nM on Jurkat cells that could be evidence that toxic action mechanisms of r-tamapin and apamin are distinct. Viability graphs of HBP lymphocytes (E,F) were normalized in order for the effect of the naturally dying cells to not be considered. For clarity, scale of viability graphs on HPB lymphocytes are displayed from 70 to 100%, due to the small effect on these cells.

Table 3. IC_{50} of All Assayed Peptides

peptide	apamin	r-tamapin	GS-tamapin	r-R6A	r-R13A	r-R6A-R7A	GS-R7A
IC_{50} [nM]	15.3	13.6	15.5	18.2	19.7	23.6	27.3

dead cells, although more studies are needed to confirm this hypothesis.

IC_{50} values on Jurkat cells calculated for each tested peptide and apamin are presented in Table 3. r-Tamapin was the most toxic peptide (IC_{50} = 13.6 nM), while mutations reduced its toxicity to a maximum IC_{50} of 27.3 nM in the case of GS-R7A. All our RXA mutants showed lower toxicity than the peptide with the native sequence; however, the IC_{50} values stayed in the nanomolar range, even in the case of the double mutant. These slight variations in the IC_{50} values suggest that the cytotoxicity is barely affected by modifications in the arginine residues 6, 7, and 13. To corroborate these results, we performed cytotoxicity assays on MDA-MB-231 cells, which also express KCa2.2 channels; interestingly, the viability curves displayed a similar behavior (Figures 4C,D and S1-J, Supporting Information). The IC_{50} of r-tamapin, apamin, and r-R7A are 0.9, 0.7, and 2.5 nM, respectively, on MDA-MB-231 cells. Although r-tamapin IC_{50} on this cell line was approximately 15 times smaller than that on Jurkat cells, the least active peptide, when compared to r-tamapin, has IC_{50} values two times smaller on both MDA-MB-231 and Jurkat cells.

Mechanism of Cell Death. The mechanism of cell death was determined by flow cytometry analysis with the FITC Annexin V Apoptosis Detection Kit with PI (Biolegend, USA); r-R7A, r-tamapin, and apamin were analyzed. Results are in the Supporting Information (Figures S4 and S5, and Tables S2 and S3). For the cultures of Jurkat T cells E6-1, the most important effect was observed with r-tamapin. In this case, an apoptotic cell death pathway was principally observed with a 69.1% at the higher dose and 36 h of exposure. The activity of r-tamapin is nearly equal to the activity of apamin, which presents 67.8% of apoptosis on the same conditions. The peptide r-R7A was the least active compared with apamin and r-tamapin and just presented 46.4% of apoptosis in Jurkat T cell cultures. These results correlate with those found for stains with CFDA and PI. In the case of MDA-MB-231 cell cultures, the mechanism of death was principally apoptotic when cultures were treated with r-tamapin, apamin, and r-R7A. Apamin showed the greatest activity against MDA-MB-231 cells with 58.7% of apoptosis, followed by r-tamapin with 57.7%, and finally r-R7A with 53.8%. It is important to note that there were never more than 2.1% of necrotic cells in either culture for all assayed treatments.

Structure–Activity Relationship. The choice for the *in vitro* model used in this work is based on two facts. First, channel blocking by toxins reduces proliferation in several cancer cell lines (reviewed in ref 35); for example, blocking KCa channels produces growth inhibition in human melanoma

dx.doi.org/10.1021/tx4004193 | *Chem. Res. Toxicol.* 2014, 27, 960–967

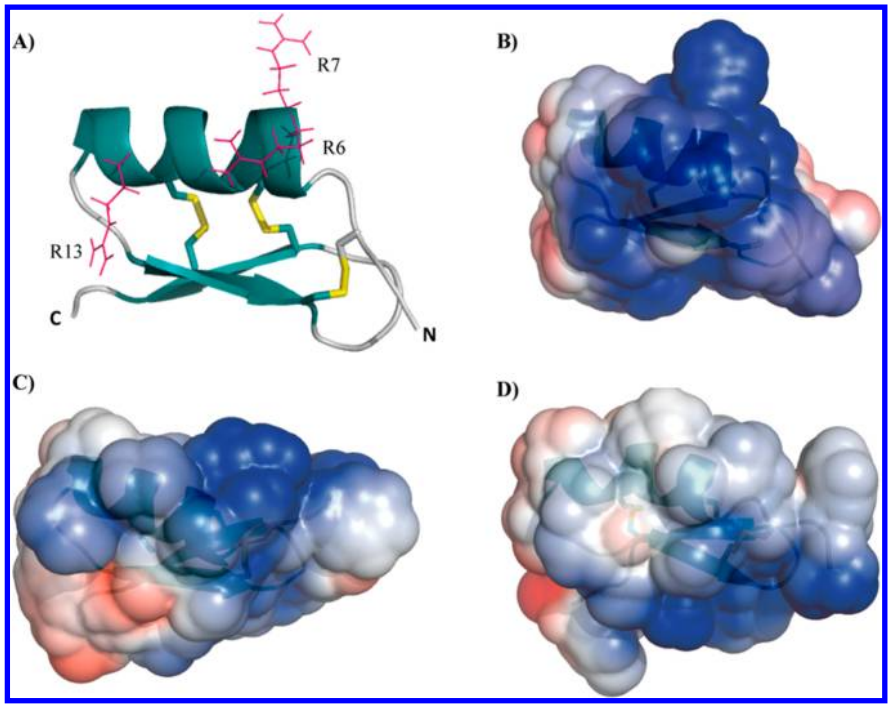

Figure 5. (A) Cartoon representation of r-tamapin. Side chain of arginines 6, 7, and 13 are shown in pink lines, and disulfide bridges are colored yellow. Electrostatic potential surface of r-tamapin (B), r-R6A (C), and r-R6A-R7A (D) displayed with a scale from −2 to 2 kBT/ec. Cartoon representations are embedded in the electrostatic potential surfaces. The orientation of the surfaces is the same as that in panel A. Decrement of positive charge density in the α helix region produced by mutations are evidenced.

cells;[36] a mechanism that connects ion channels with the cell cycle is still under discussion, but it is thought to be related to Ca^{2+} homeostasis. In Jurkat cells, KCa2.2 channel blockage causes membrane depolarization and inhibits Ca^{2+} entry.[37] Second, the Jurkat leukemic T cell line constitutively expresses two K^+ channels: a voltage-gated one ($K_V1.3$) and a small conductance Ca^{2+} activated one, the KCa2.2 channel,[17,38] which is also found in MDA-MB-231 cells.[39] Therefore, these two lines are good models to test peptide toxicities due to KCa channel blocking.

Our activity assays on HPB lymphocytes showed low toxicity for all described peptides. Assays were performed at pH 7, so arginine residues must be positively charged. The total charge of r-tamapin under these conditions is 2+, while single mutants have 1+ charge, and the double mutant r-R6A-R7A is neutral. Viability curves on HPB lymphocytes (Figures 4E,F and S1F−I, Supporting Information) showed that peptides had a minimal time-dependent toxic effect. On these assays, only GS-R7A presented a slight concentration-dependent toxicity (Figure 4F). This mutant has the maximum toxicity of all assayed peptides (20% at 100 nM). There is no correlation between the peptide total charge and its activity; for example, GS-R7A, with 1+ charge, showed a higher toxic effect than both of the double charged peptides, r-tamapin and GS-tamapin. Additionally, apamin revealed a slow toxicity and a similar behavior compared to that of tamapin mutants on HPB lymphocytes (Supporting Information). Altogether, these results evidence the lack of correlation between charge and activity, thus suggesting a poor electrostatic interaction between peptides and cells.

In contrast, the assays on the Jurkat T cell line show that the toxicity of all peptides is strongly concentration-dependent (Figures 4A,B and S1A−E, Supporting Information) and tends to increase with the peptide's charge. Peptides with similar total charge had slight differences in their toxic activities. For example, r-R6A and r-R13A, whose total charge is 1+, have IC_{50} values of 18.2 nM and 19.7 nM, respectively, while r-tamapin, whose total charge is 2+, has IC_{50} = 13.6, and r-R6A-R7A, which has no charge in the assayed conditions, has IC_{50} = 23.6. These differences suggest that the mechanism responsible for peptide toxicity is determined by electrostatic and possibly specific interactions. To support this idea, we determined the electrostatic potential surfaces of all assayed peptides. These maps reveal substantial differences among the single RXA mutants (Figure 5C,D). Electrostatic surfaces of both r-R6A and r-R13A exhibit a reduced positive zone when compared to the r-tamapin's widespread positive potential surface. Similarly, the double mutant r-R6A-R7A displays a reduced charged potential surface on the putative interaction zone; surprisingly, this peptide's activity is similar to the single or native peptides' activity but is less active than GS-R7A. The tridimensional structures of all tested peptides are superimposable, as shown in Figure 3B, where even when the mutations are present, the side chains surrounding the interaction zone are exposed. It is important to remark that the alanine mutations we introduced do not present steric hindrance for interactions with residues in the vicinity; thus, if interaction with the cell is not directly related to mutated sites, toxicity should have minimal effect, as we observed in our assays. Apamin, which has an IC_{50} value close to that of r-tamapin in both Jurkat and MDA-MB-231 cells, produces similar viability curves (Figure 4B and D). Besides, both toxins produce cell death by apoptosis, thus suggesting that both peptides act through a similar mechanism. Previous reports have determined that apamin interacts with KCa2.2 channels through the S3−S4 extracellular loop and the outer pore of an adjacent subunit,[40] but the exact blocking mechanism has not been detailed for tamapin, even though a simple pore block has been proposed.[41] Similitudes in our

dx.doi.org/10.1021/tx4004193 | Chem. Res. Toxicol. 2014, 27, 960−967

results using two different cell lines that express KCa2.2 channels strongly suggest that the toxicity mechanism involves interaction with these macromolecules. In contrast to the RXA mutants, GS-peptides presented lower activity than their analogues with no additional residues; this suggests that longer amino termini may cause difficulties in the interaction with cells. Our results also suggest that tamapin's toxicity mechanism is due to the global structure of the toxin rather than being due to specific interactions between the arginine residues and the cells. Besides, a comparison was made between those cells that express KCa2.2 channels and those that do not, and it was found that the latter live longer. Together, these results suggest that the toxicity of r-tamapin and its mutants is specific to cells with KCa2.2 channels.

■ CONCLUSIONS

This work provides important evidence regarding the toxicity of tamapin in living cells. r-Tamapin and its mutants display a selective cytotoxic activity, producing apoptosis on Jurkat T and MDA-MB-231 cells, which constitutively express KCa2.2 channels, with IC_{50} values in the nanomolar range, whereas they have only minimal effects on HPB lymphocytes, which do not express KCa2.2 channels. These results are evidence of the pharmacological potential of tamapin as a proliferation inhibitor of KCa2.2 expressing T cells with no effect on common T lymphocytes. Modifications in the toxin's primary sequence changed its lethality when assayed on Jurkat T and MDA-MB-231 cells. Mutations of arginine residues by alanine in positions 6, 7, and 13 produced peptides with decreased activity, thus suggesting that these residues are involved in the activity mechanism. The minimal reduction of IC_{50} values may be due to compensatory mechanisms or allosteric effects; future work should help to confirm this idea.

■ ASSOCIATED CONTENT

Supporting Information

Viability graphics of HBP and Jurkat lymphocytes in the presence of the peptides R6A, R13A, R6A-R7A, and GS-R7A, as well as viability graphs of MDA-MB-231 cells in the presence of r-tamapin, R7A, and apamin, Ramachandran plot of GS-R7A, electrostatic surface potential of R13A and R7A, dot plots of cytometry assays on Jurkat cells and on MDA-MB-231 cells, table of averaged values of viability assays performed on Jurkat E6-1 cells, and cytometric results on Jurkat E6-1 and on MDA-MB-231 cells. This material is available free of charge via the Internet at http://pubs.acs.org.

Accession Codes

NMR assignments and coordinates have been deposited in BioMagResBank and the Protein Data Bank with entries r-tamapin (2LU9:18513), GS-tamapin (2KY3:17227), GS-R6A (19519:2ME7), GS-R7A (19524:2MEL), GS-R13A (19527:2MEN), and GS-R6A-R7A (19528:2MEO).

■ AUTHOR INFORMATION

Corresponding Author

*Phone: +52-55-56224613. Fax: +52-55-56162203. E-mail: jfrp@unam.mx.

Present Address

‖(R.H.-L.) Department of Chemistry and Chemical Biology, Harvard University, 12 Oxford Street, Cambridge, MA 02138.

Funding

This work was partially supported by the Consejo Nacional de Ciencia y Tecnología (CONACYT), Mexican Government (Grants 59297 and 166472), and Dirección General de Asuntos del Personal Académico (DGAPA)-UNAM, project IN205110 and IN207713.

Notes

The authors declare no competing financial interest.

■ ACKNOWLEDGMENTS

B.R.-C., D.F.-S., A.L.S., and R.H.-L. want to thank CONACyT for the scholarships. R.H.-L. thanks Fundación Harvard Mexico for the scholarship. B.R.-C. wants to thank Andrea Cabrera for helpful discussions and support and Gustavo Titaux for the TOC. We are ever so grateful toward the reviewers for their positive criticism and suggestions.

■ ABBREVIATIONS

DQF-COSY, double quantum filtered correlated spectroscopy; DPFGSE, double pulsed field gradient spin echo; TOCSY, total correlation spectroscopy; NOE, nuclear Overhauser effect; NOESY, NOE spectroscopy; KCa2.2, calcium activated K^+ channels, subtype 2.2; RMSD, root-mean-square deviation; IMAC, immobilized metal ion affinity chromatography; Trx, thioredoxin

■ REFERENCES

(1) Rodríguez de la Vega, R. C., Schwartz, E. F., and Possani, L. D. (2010) Mining on scorpion venom biodiversity. *Toxicon 56*, 1155−1161.

(2) Billen, B., Bosmans, F., and Tytgat, J. (2008) Animal peptides targeting voltage-activated sodium channels. *Curr. Pharm. Des. 14*, 2492−2502.

(3) Mouhat, S., Andreotti, N., Jouirou, B., and Sabatier, J. M. (2008) Animal toxins acting on voltage-gated potassium channels. *Curr. Pharm. Des. 14*, 2503−2518.

(4) Tytgat, J., Chandy, K. G., Garcia, M. L., Gutman, G. A., Marti-Euclaire, M. F., van der Walt, J. J., and Possani, L. D. (1999) A unified nomenclature for short-chain peptides isolated from scorpion venoms: alpha-KTx molecular subfamilies. *Trends Pharmacol. Sci. 20*, 444−447.

(5) Pedarzani, P., Dhoedt, D., Doorty, K. B., Wadsworth, J. D. F., Jhosep, J. S., Jeyaseelan, K., Kini, R. M., Gadre, S. V., Sapatnekar, S. M., Stocker, M., and Strong, P. N. (2002) Tamapin, a venom peptide from the Indian red scorpion (*Mesobuthus tamulus*) that targets small conductance Ca^{2+}-activated K^+ channels and afterhyperpolarization currents in central neurons. *J. Biol. Chem. 277*, 46101−46109.

(6) Bond, C. T., Maylie, J., and Adelman, J. P. (2005) SK channels in excitability, pace making and synaptic integration. *Curr. Opin. Neurobiol. 15*, 305−311.

(7) Stocker, M., Krause, M., and Pedarzani, P. (1999) An apamin-sensitive Ca^{2+}-activated K^+ current in hippocampal pyramidal neurons. *Proc. Natl. Acad. Sci. U.S.A. 96*, 4662−4667.

(8) Weatherall, K. L., Goodchild, S. J., Jane, D. E., and Marrion, N. V. (2010) Small conductance calcium-activated potassium channels: From structure to function. *Prog. Neurobiol. 91*, 242−255.

(9) Shakkottai, V. G., Regayas, I., Wulff, H., Fajloun, Z., Tomita, H., Fathallah, M., Cahalan, M. D., Gargus, J. J., Sabatier, J. M., and Chandy, K. G. (2001) Design and characterization of a highly selective peptide inhibitor of the small conductance calcium-activated K^+ channel, SkCa2. *J. Biol. Chem. 276*, 43154−43151.

(10) Wu, J. J., He, L. L., Zhou, Z., and Chi, C. W. (2002) Gene expression, mutation, and structure-function relationship of scorpion toxin BmP05 active on SKCa channels. *Biochemistry 41*, 2844−2849.

(11) Sabatier, J. M., Zerrouk, H., Darbon, H., Mabrouk, K., Benslimane, A., Rochat, H., Martin-Euclaire, M. F., and Van Rietschoten, J. (1993) P05, a new leiurotoxin I-like scorpion toxin:

synthesis and structure-activity relationship of the alpha-amidated analog, a ligand of Ca^{2+} activated K^+ channels with increased affinity. *Biochemistry 32*, 2763−2770.
(12) Martins, J. C., Van de Ven, F. J., and Borremans, F. A. (1995) Determination of the three-dimensional solution structure of scyllatoxin by ^1H nuclear magnetic resonance. *J. Mol. Biol. 253*, 590−603.
(13) Lecomte, C., Ferrat, G., Fajloun, Z., Van Rietschoten, J., Rochat, H., Martin-Eauclaire, M. F., Darbon, H., and Sabatier, J. M. (1999) Chemical synthesis and structure-activity relationship of Ts *κ*, a novel scorpion toxin acting on apamin-sensitive SK channel. *J. Pept. Res. 54*, 369−376.
(14) Cui, M., Shen, J., Briggs, J. M., Fu, W., Wu, J., Zhang, Y., Luo, X., Chi, Z., Ji, R., Jiang, H., and Chen, K. (2002) Brownian dynamics of the recognition of the scorpion toxin P05 with small conductance calcium-activated potassium channels. *J. Mol. Biol. 318*, 417−428.
(15) Andreotti, N., di-Luccio, E., Sampieri, F., Waard, M., and Sabatier, J. M. (2005) Molecular modeling and docking simulations of scorpion toxins and related analogs on human SKCa2 and SKCa3 channels. *Peptides 26*, 1095−1108.
(16) Pedarzani, P., and Stocker, M. (2008) Molecular and cellular basis of small- and intermediate-conductance, calcium-activated potassium channel function in the brain. *Cell Mol. Life. Sci. 65*, 3196−3217.
(17) Jäger, H., Adelman, J. P., and Grissmer, S. (2000) SK2 encodes the apamin-sensitive Ca^{2+}-activated K^+ channels in the human leukemic T cell line, Jurkat. *FEBS Lett. 469*, 196−202.
(18) Zhao, D. X., Ding, Z. C., Liu, Y. Q., and Huang, Z. X. (2007) Overexpression and purification of a single zinc finger peptides of human zinc finger protein ZNF191. *Protein Expression Purif. 53*, 232−237.
(19) Gobom, J., Schuerenberg, M., Mueller, M., Theiss, D., Lehrach, H., and Nordhoff, E. (2001) *α*-Cyano-4-hydroxycinnamic acid affinity sample preparation. A protocol for MALDI-MS peptide analysis in proteomics. *Anal. Chem. 73*, 434−438.
(20) Hwang, T. L., and Shaka, A. J. (1995) Water suppression that works. Excitation sculpting using arbitrary waveforms and pulsed field gradients. *J. Magn. Reson. 112*, 275−279.
(21) Delaglio, F., Grzesiek, S., Vuister, G. W., Zhu, G., Pfeifer, J., and Bax, A. (1995) NMRPipe. A multidimensional spectral pro-cessing system based on UNIX pipes. *J. Biomol. NMR 6*, 277−293.
(22) Bartels, C., Xia, T., Billeter, M., Güntert, P., and Wüthrich, K. (1995) The program XEASY for computer-supported NMR spectral analysis of biological macromolecules. *J. Biomol. NMR 6*, 1−10.
(23) Wagner, G., and Wüthrich, K. (1982) Sequential resonance assignments in protein ^1H nuclear magnetic resonance spectra. Basic pancreatic trypsin inhibitor. *J. Mol. Biol. 155*, 347−366.
(24) Gunter, P. (2004) Automated NMR structure calculation with CYANA. *Methods Mol. Biol. 278*, 353−378.
(25) Herrmann, T., Günter, P., and Wuthrich, K. (2002) Protein NMR structure determination with automated NOE assignment using the new software CANDID and the torsion angle dynamics algorithm DYANA. *J. Mol. Biol. 319*, 209−227.
(26) Case, D. A., Darden, T. A., Cheatham, T. E., III, Simmerling, C. L., Wang, J., Duke, R. E., Luo, R., Merz, K. M., Pearlman, M. A., Crowley, M., Walker, R. C., Zhang, W., Wang, B., Hayik, S., Roitberg, A., Seabra, G., Wong, K. F., Paesani, F., Wu, X., Brozell, S., Tsui, V., Gohlke, H., Yang, L., Tan, C., Mongan, J., Hornak, V., Cui, G., Beroza, P., Mathews, D. H., Schafmeister, C., Ross, W. S., and Kollman, P. A. (2006) *AMBER 9*, University of California, San Francisco, CA.
(27) Berendsen, H. J. C., Postma, J. P. M., van Gunsteren, W. F., Dinola, A., and Haak, J. R. (1984) Molecular dynamics with coupling to an external bath. *J. Chem. Phys. 81*, 3684−3690.
(28) Jorgensen, W. L., Chandrasekhar, J., Madura, J., and Klein, M. L. (1983) Comparison of simple potential functions for simulating liquid water. *J. Chem. Phys. 79*, 926−935.
(29) Hornak, V., Abel, R., Okur, A., Strockbine, B., Roitberg, A., and Simmerling, C. (2006) Comparison of multiple AMBER force fields and development of improved protein backbone parameters. *Proteins 65*, 712−725.
(30) Gurrola, G. B., Hernández-López, R. A., Rodríguez de la Vega, R. C., Varga, Z., Batista, C. V. F., Salas-Castillo, S. P., Panyi, G., and del Río-Portilla, F. (2012) Structure, function and chemical of Vaejovis mexicanus peptide 24: A novel potent blocker of Kv1.3 potassium channels of human T lymphocytes. *Biochemistry 51*, 4049−4061.
(31) Gasteiger, E., Hoogland, C., Gattiker, A., Duvaud, S., Wil-kins, M. R., Appel, R. D., and Bairoch, A. (2005) Protein Identification and Analysis Tools on the ExPASy Server. *The Proteomics Protocols Handbook*, 2nd ed., pp 571−607, Humana Press, Totowa, NJ.
(32) Davaux, C., Knibiehler, M., Defendini, M.-L., Mabrouk, K., Rochat, H., van Rietschoten, J., Baty, D., and Granier, C. (1995) Recombinant and chemical derivatives of apamin. Implicationof post-transcriptional C-terminal amidation of apamin in biological activity. *Eur. J. Biochem. 231*, 544−550.
(33) Meunier, S., Bernassau, J. M., Sabatier, J. M., Martin-Eauclaire, M. F., Van Rietschoten, J., Cambillau, C., and Darbon, H. (1993) Solution structure of P05-NH_2, a scorpion toxin analog with high affinity for the apamin-sensitive potassium channel. *Biochemistry 32*, 11969−11976.
(34) Feske, S., Skolnik, E. Y., and Prakriya, M. (2012) Ion channels and transporters in lymphocyte function and immunity. *Nat. Rev. Immunol. 12*, 532−547.
(35) Girault, A., Haelters, J. P., Potier-Cartereau, M., Chantôme, A., Jaffrés, P. A., Bougnoux, P., Joulin, V., and Vandier, C. (2012) Targeting SKCa channels in cancer: potential new therapeutic approaches. *Curr. Med. Chem. 19*, 697−713.
(36) Tajima, N., Schönherr, K., Niedling, S., Kaatz, M., Kanno, H., Schönherr, R., and Heinemann, S. H. (2006) Ca^{2+}-activated K^+ channels in human melanoma cells are up-regulated by hypoxia involving hypoxia-inducible factor -1α and the von Hippel-Lindau protein. *J. Physiol. 571*, 349−359.
(37) Fanger, C., Rauer, H., Neben, A. L., Miller, M. J., Rauer, H., Wulff, H., Campos, J., Ganellin, C. R., Chandy, K. G., and Calahan, M. D. (2001) Calcium-activated potassium channels sustain calcium signaling in T lymphocytes. *J. Biol. Chem. 276*, 12249−12256.
(38) Desai, R., Peretz, A., Idelson, H., Lazarovici, P., and Attali, B. (2000) Ca^{2+}-activated K^+ channels in human leukemic Jurkat T cells. Molecular cloning, biochemical and functional characterization. *J. Biol. Chem. 275*, 39954−39963.
(39) Potier, M., Joulin, V., Roger, S., Besson, P., Jourdan, M.-L., LeGuennec, J.-Y., Bougnoux, P., and Vandier, C. (2006) Identification of SK3 channel as a new mediator of breast cancer cell migration. *Mol. Cancer Ther. 5*, 2946−2953.
(40) Weatherall, K. L., Seutin, V., Liégeois, J.-F., and Marrion, N. V. (2011) Crucial role of a shared extracellular loop in apamin sensitivity and maintenance of pore shape of small conductance calcium-activated potassium (SK) channels. *Proc. Natl. Acad. Sci. U.S.A. 108*, 18494−18499.
(41) Rodríguez de la Vega, R. C., Merino, E., Becerril, B., and Possani, L. D. (2003) Novel interactions between K^+ channels and scorpion toxins. *Trends Pharmacol. Sci. 24*, 222−227.